

# Theory of double resonance magnetometers based on atomic alignment

Antoine Weis\* and Georg Bison

*Physics Department, University of Fribourg,  
Chemin du Musée 3, 1700 Fribourg, Switzerland*

(Dated: May 26, 2006)

## Abstract

We present a theoretical study of the spectra produced by optical/radio-frequency double resonance devices, in which resonant *linearly* polarized light is used in the optical pumping and detection processes. We extend previous work by presenting algebraic results which are valid for atomic states with arbitrary angular momenta, arbitrary rf intensities, and arbitrary geometries. The only restriction made is the assumption of low light intensity. The results are discussed in view of their use in optical magnetometers.

PACS numbers: 32.60.+i, 32.30.Dx, 07.55.Ge, 33.40.+f

---

\*Electronic address: antoine.weis@unifr.ch

## I. INTRODUCTION

Since the 1950s the combination of resonant optical excitation and magnetic resonance has been an extremely valuable tool for atomic spectroscopy. This double resonance technique [1] has not only proven useful for investigating atomic structure, for measuring properties of atoms, their constituents, and their interactions, but has also led to important applications in atom cooling, optically pumped frequency standards, and optical magnetometers.

Magnetometers based on double resonance in atomic samples measure the modulus of an externally applied magnetic field  $\mathbf{B}_0$  via the Larmor precession frequency of the sample's magnetization in that field [2, 3]. The sample is typically a vapor of paramagnetic atoms (or diamagnetic atoms excited to a metastable state with an orbital angular momentum) sealed in a glass cell. A macroscopic magnetization is created in the vapor by optical pumping with polarized resonance radiation. The magnetization precesses in the magnetic field  $\mathbf{B}_0$  to be measured (referred to as the offset field) and that precession is driven by a (much weaker) magnetic field  $\mathbf{B}_1(t)$  (referred to as the rf field), co-rotating with the magnetization around the offset field.

Since the optical properties of the medium, characterized by its complex index of refraction, depend on its spin polarization, the driven magnetization will induce periodic modulations of those properties [4, 5], which are then detected. In most applications, the same light beam used to polarize the medium is also used to monitor the oscillations by measuring either the power or the polarization state of the transmitted beam. The frequency of the induced oscillations coincides with the oscillation frequency  $\omega$  of the rf field, and their amplitude depends in a resonant way on the detuning between  $\omega$  and the Larmor frequency  $\omega_0 = \gamma_F B_0$  associated with the offset field. The Landé factor  $\gamma_F = g_F \mu_B / \hbar$  is characteristic for the pumped atomic state with total angular momentum  $F$ .

Most practical double resonance devices rely on atomic orientation prepared by optical pumping with *circularly* polarized light. In this paper we present a theoretical study of the resonance signals obtained in double resonance spectroscopy using *linearly* polarized light. As shown first by Bell and Bloom [6] magnetic resonance in aligned media leads to signal modulations at the fundamental and at the second harmonic of the rf frequency. We derive algebraic expressions for the spectral line shapes of the in-phase and quadrature components of both signals and their orientation dependence. Previous theoretical treatments of such

signals [7, 8] were restricted to specific angular momentum states ( $J = 1$ ) or to low rf powers. The results presented here are more general in the sense that they apply to arbitrary spin systems and that they are valid for arbitrary rf power levels and for arbitrary orientations of  $\mathbf{B}_0$  with respect to the light polarization.

## II. POLARIZED ATOMIC MEDIA

### A. Atomic Multipole Moments

The density matrix  $\rho$  of an ensemble of polarized atoms with angular momentum  $F$  can be expressed in terms of atomic multipole moments  $m_{k,q}$  according to [9]

$$\rho = \sum_{k=0}^{2F} \sum_{q=-k}^k m_{k,q} T_q^{(k)}, \quad (1)$$

where the  $T_q^{(k)}$  are standard irreducible tensor operators

$$T_q^{(k)}(F) = \sum_{M=-F}^F \sum_{M'=-F}^F (-1)^{F-M'} \times \langle F, M, F, -M' | k, q \rangle |F, M\rangle \langle F, M'| \quad (2)$$

constructed from the angular momentum states  $|F, M\rangle$ , and where the multipole moments  $m_{k,q}$  are defined by

$$m_{k,q} = \langle T_q^{(k)\dagger} \rangle = \text{Tr}(\rho T_q^{(k)\dagger}). \quad (3)$$

The three multipole moments  $m_{k=1,q=-1,0,+1}$  represent the orientation of the medium, while the five components  $m_{k=2,q=-2,\dots,+2}$  represent its alignment. The multipole moments  $m_{k,q=0}$  are called longitudinal multipole moments and their value depends only on sublevel populations. The multipole moments  $m_{k,q \neq 0}$  represent sublevel coherences and are called transverse moments. The representation of the atomic polarization in terms of multipole moments has a significant advantage over a representation in terms of sublevel populations and coherences. In principle, both representations require the same number of parameters for the complete description of the atomic ensemble. However, because electric dipole radiation couples only [10] to orientation ( $k = 1$ ) and alignment ( $k = 2$ ) it is sufficient to specify the corresponding  $3 + 5 = 8$  multipole moments for the complete description of the system's optical properties. Moreover, specific light polarizations couple only to specific subsets of

these 8 multipole moments, so that the use of the tensor formalism in systems with large angular momenta leads to a significant simplification of the mathematical treatment. In the case discussed here only the (real) multipole moment  $m_{2,0}$  will be relevant. This approach therefore allows one to derive results valid for systems with arbitrary angular momenta.

A resonant *circularly* polarized laser beam interacting with an unpolarized atomic sample will create orientation ( $k = 1$ , vector polarization) and alignment ( $k = 2$ , tensor polarization) in the sample by optical pumping. The lowest order multipole that a *linearly* polarized light field can create is an atomic alignment. While only atomic states with  $J \geq 1/2$  can be oriented, the condition  $J \geq 1$  has to be fulfilled for the creation of an aligned state. Note that an alignment along the direction of light propagation can also be produced by pumping with *unpolarized* light [6, 11]. The ground state of alkali atoms has an electronic angular momentum  $J = 1/2$ , which cannot be aligned. However, the hyperfine interaction with the nuclear spin splits the ground state into two hyperfine levels with total angular momenta  $F_{\pm} = I \pm J$ , which can be aligned provided  $F \geq 1$ . An alignment can therefore be prepared and/or detected only if the light source has a sufficient spectral resolution to excite a single hyperfine transition. In general the Doppler (and pressure) broadened spectra of discharge lamps, used in conventional optically pumped magnetometers (OPM), cannot be used to address individual hyperfine lines and hence do not allow one to create nor to detect a ground state alignment. However, radiation from a narrowband laser can resolve the hyperfine structure and it is well known that a linearly polarized laser beam can create an atomic alignment.

## B. DROMs and DRAMs

We will refer to an OPM based on atomic orientation as DROM (double resonance orientation magnetometer), while we will speak of DRAM (double resonance alignment magnetometer) when the magnetization has the symmetry of an atomic alignment. Most of the past research work on double resonance spectroscopy dealt with oriented vapors, although alignment induced by (unpolarized) lamp pumping in  $J = 1$  metastable states of  $^4\text{He}$  was already reported in 1960/61 [6, 11]. In alkali atoms, alignment produced by lamp pumping can be observed using line splitting by the quadratic Zeeman effect [12] or isotope filtering [5, 12]. The latter technique is, however, restricted to Rb and cannot be applied to other

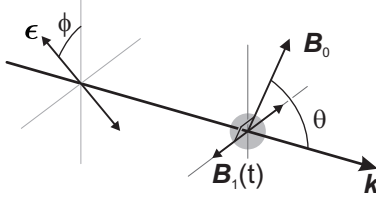


FIG. 1: Geometry of double resonance spectroscopy involving light with a linear polarization vector  $\epsilon$  and a wave vector  $\mathbf{k}$ . The oscillating field  $\mathbf{B}_1$  is perpendicular to the offset field  $\mathbf{B}_0$ .

alkalis. As mentioned above, linearly polarized laser radiation is an efficient means for producing alignment and a discussion of linearly polarized laser pumping in metastable  $^4\text{He}$  can be found in [7, 13]. These authors have investigated several magnetometry techniques using both orientation and alignment signals and they observed magnetic resonances involving alignment using rf fields, light intensity modulation, polarization modulation, and frequency modulation. A variant of the latter technique – in which the transmitted lights’ polarization, instead of intensity, was measured – was realized with  $^{87}\text{Rb}$  [14, 15].

### III. DRAM GEOMETRY

We will restrict the discussion to geometries in which the rf field  $\mathbf{B}_1$  is perpendicular to the offset field  $\mathbf{B}_0$ . With this condition, the possible geometries of a double resonance experiment with linearly polarized light can be described in terms of two angular parameters, viz.,  $\theta$ , the angle between  $\hat{B}_0$  and the propagation direction  $\hat{k}$  of the laser beam, and  $\phi$ , the angle between the light polarization  $\hat{\epsilon}$  and the plane spanned by  $\hat{B}_0$  and  $\hat{k}$  (Fig. 1). Because the signals are independent of the orientation  $\hat{k}$ , the geometry of the problem is fully determined by  $\hat{B}_0$ ,  $\hat{B}_1$ , and  $\hat{\epsilon}$  so that one can consider the equivalent parametrization shown in Fig. 2, in which  $\gamma$  denotes the angle between the offset field and the light polarization [8]. The orientation dependence of the signal amplitudes will be determined by this single angular parameter, while the polar angle  $\alpha$  will lead to a phase shift in the time dependence of the oscillating signals (Sec. VI). In the calculation presented below we will therefore consider only the geometry depicted in Fig. 2.

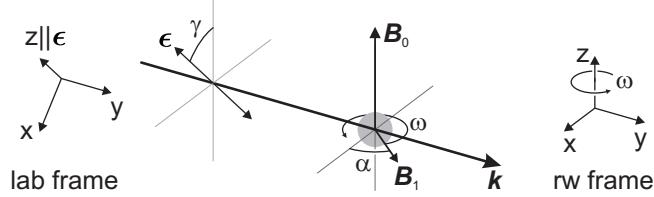


FIG. 2: Alternative parametrization of the DRAM geometry, in which  $\mathbf{B}_1$  is perpendicular to  $\mathbf{B}_0$ . The rotating wave (rw) frame and the rotating magnetic field  $\mathbf{B}_1$  are shown for one particular moment in time.

#### IV. MODEL CALCULATIONS

In Fig. 2 we have applied the rotating wave approximation by decomposing the rf field into two counter-rotating fields, from which we have retained only the component co-rotating with the alignment. This component is shown in its position at time  $t = 0$ , thereby defining the time origin of the phases of the oscillating signal components. The magnetometer signals are calculated following a 3-step (prepare, evolve, probe) approach [16].

##### A. Step 1: Creation of alignment by optical pumping

For the description of the pumping process we chose a coordinate frame in which the quantization axis lies along the light polarization (lab frame in Fig. 2). For symmetry reasons, the only non-vanishing alignment component created by the optical pumping process is the longitudinal multipole moment

$$m_{2,0}^{\text{ini}} = N_2(F) \sum_{M=-F}^F p_M [3M^2 - F(F+1)] ,$$

expressed in terms of the sublevel populations  $p_M$  and a normalization constant  $N_2(F)$ [9]. In the presence of an offset field  $\mathbf{B}_0$  the alignment components perpendicular to  $\mathbf{B}_0$  will relax to zero yielding a steady state value of

$$m_{2,0}^{\text{eq}} = m_{2,0}^{\text{ini}} \frac{3 \cos^2 \gamma - 1}{2} \quad (4)$$

for the alignment along the magnetic field, given by the projection of  $m_{2,0}^{\text{ini}}$  on the field direction. Note that this steady state is reached only when the Larmor frequency is much larger than the transverse relaxation rates. This condition is well fulfilled for high- $Q$  magnetic

resonances while it is not met by zero-field level-crossing resonances (ground state Hanle effect, nonlinear Faraday effect[16]).

## B. Step 2: Magnetic resonance

This step describes the magnetic resonance process, i.e., the evolution of the alignment under the combined actions of the magnetic fields  $\mathbf{B}_0$ ,  $\mathbf{B}_1$ , and relaxation processes. It is described in a coordinate frame, which is related to the lab frame by a static rotation of  $-\gamma$  around the  $y$ -axis and then by a dynamic rotation, at the frequency  $\omega$ , around the new  $z$ -axis. In this frame, which we call the rotating wave frame (rw frame), the offset field  $\mathbf{B}_0$  is along  $z$ , while the rf field  $\mathbf{B}_1$  appears to be static and oriented at an angle  $\alpha$  with respect to the  $x$ -direction (see Fig 2). This is the usual field configuration for describing magnetic resonance processes. Note that  $m_{2,0}^{\text{eq}}$  is not affected by the transformation to the rw frame. Due to the rotation of the coordinate frame, a fictitious magnetic field  $\mathbf{B}_f = -\omega\hat{z}/\gamma_F$  appears in the rw frame, and the atoms see a total field  $\mathbf{B}_{\text{tot}} = B_1 \cos \alpha \hat{x} + B_1 \sin \alpha \hat{y} + (B_0 - \omega/\gamma)\hat{z}$ .

The evolution of the the system's density matrix is described by the Liouville equation

$$\frac{d}{dt}\rho = \frac{1}{\hbar i} [H, \rho] - \rho_{\text{relax}}, \quad (5)$$

with  $H = -\boldsymbol{\mu} \cdot \mathbf{B}_{\text{tot}}$ , and where  $\rho_{\text{relax}}$  describes the relaxation processes. Inserting the multipole decomposition (1) into (5) yields the following equations of motion for the multipole moments  $m_{2,q}$

$$\frac{d}{dt}m_{2,q} = \sum_{q'} \mathbb{O}_{qq'}^{(2)} m_{2,q'} - m_{2,q}^{\text{relax}} \quad q = -2, -1, \dots, 2, \quad (6)$$

where  $\mathbb{O}_{qq'}^{(2)}$  is given by

$$\mathbb{O}_{qq'}^{(2)} = \begin{pmatrix} -2i\delta & i\omega_1 p_- & 0 & 0 & 0 \\ i\omega_1 p_+ & -i\delta & i\sqrt{\frac{3}{2}}\omega_1 p_- & 0 & 0 \\ 0 & i\sqrt{\frac{3}{2}}\omega_1 p_+ & 0 & i\sqrt{\frac{3}{2}}\omega_1 p_- & 0 \\ 0 & 0 & i\sqrt{\frac{3}{2}}\omega_1 p_+ & i\delta & i\omega_1 p_- \\ 0 & 0 & 0 & i\omega_1 p_+ & 2i\delta \end{pmatrix},$$

in which  $\omega_1 = \gamma_F B_1$  is the Rabi frequency of the rf field,  $p_{\pm} = \exp(\pm i\alpha)$  are phase factors that describe the orientation of  $\omega_1$  in the  $xy$ -plane, and  $\delta = \omega - \omega_0$  is the detuning of the

radio frequency  $\omega$  with respect to the Larmor frequency  $\omega_0$ . The relaxation terms are given by

$$\begin{pmatrix} m_{2,2}^{\text{relax}} \\ m_{2,1}^{\text{relax}} \\ m_{2,0}^{\text{relax}} \\ m_{2,-1}^{\text{relax}} \\ m_{2,-2}^{\text{relax}} \end{pmatrix} = \begin{pmatrix} \Gamma_2 m_{2,2} \\ \Gamma_1 m_{2,1} \\ \Gamma_0 (m_{2,0} - m_{2,0}^{\text{eq}}) \\ \Gamma_1 m_{2,-1} \\ \Gamma_2 m_{2,-2} \end{pmatrix}. \quad (7)$$

where we assume that the multipole moments  $m_{2,q}$  relax at rates  $\Gamma_{|q|}$ . The transverse alignment components  $m_{2,q \neq 0}$  relax towards a zero value, while the longitudinal component  $m_{2,0}$  relaxes towards  $m_{2,0}^{\text{eq}}$ , introduced in step 1. Below, we present very general results for the case when all three relaxation rates are different, although it is well known that there are specific relations between those rates when the relaxation mechanism has specific rotational symmetries [17]. Equations 6 are a generalization of the well known Bloch equations

$$\frac{d}{dt} m_{1q} = \sum_{q'} \mathbb{O}_{qq'}^{(1)} m_{1q'} - m_{1,q}^{\text{relax}} \quad q = -1, 0, 1, \quad (8)$$

describing the evolution of the three orientation components  $m_{1,q}$ .

We have used a computer algebra software to determine algebraic expressions for the steady state ( $d/dt m_{2,q} = 0$ ) solutions  $m_{2,q}$  of (6). These solutions are then transformed back to the lab frame, by first applying a dynamic rotation at the rate  $-\omega$  around the  $z$ -axis, and then a static rotation by  $\gamma$  around the  $y$ -axis of the rw frame. In this way one can derive algebraic expressions for the time dependent multipole moments  $m_{2,q}(t)$  in the lab frame.

### C. Step 3: Detection of the oscillating steady state alignment

In the third and final step, we calculate the effect the time dependent multipole moments have on the optical absorption coefficient of the medium. One can show that the absorption coefficient of a medium described by  $m_{k,q}$  for linearly polarized light is proportional to

$$\kappa \propto \frac{A_0}{\sqrt{3}} m_{0,0} - \sqrt{\frac{2}{3}} A_2 m_{2,0}, \quad (9)$$

where the (analyzing power)  $A_k$  depends only on the states  $|n_g, L_g, J_g, F_g\rangle$  and  $|n_e, L_e, J_e, F_e\rangle$  coupled by the light. The multipole moments in (9) are defined with respect to a quantization

axis oriented along the incident light polarization, which is the case in the lab frame, i.e., the frame in which the results of step 2 are expressed. The monopole moment  $m_{0,0}$  describes the total population of the hyperfine ground state  $|n_g, L_g, J_g, F_g\rangle$ . We assume the optical transition to be closed and the light intensity to be so weak that excited state populations remain negligible, so that the monopole moment does not depend on time. The only time dependent (oscillating) component of the absorption coefficient is therefore proportional to  $m_{2,0}(t)$ . We define the time dependent DRAM signal, normalized to the longitudinal alignment initially produced by the optical pumping, as

$$S(t) = \frac{m_{2,0}(t)}{m_{2,0}^{\text{ini}}}. \quad (10)$$

#### D. Validity of the three step approach

The three step approach is only valid if steady state conditions are reached in steps 1 and 2. This is fulfilled when the pump rate  $\Gamma_p$ , at which alignment components are modified by the interaction with the light is negligible compared to the relaxation rates  $\Gamma_{|q|}$ . This condition can be realized experimentally at low light powers, however, at the cost of a decreased signal to noise ratio. OPMs are known to perform best when  $\Gamma_p$  is comparable to  $\Gamma_{|q|}$ . The lowest order correction, taking the depolarization of light interactions into account, can be described by

$$\Gamma_{|q|} \rightarrow \Gamma_{|q|} + \Gamma_p = \Gamma_{|q|} + \eta P_L, \quad (11)$$

where  $P_L$  is the laser power.

It is well known that substitution (11) is valid to all orders in  $P_L$  for a DROM in a spin 1/2 system [18], in which orientation is the only multipole moment that can be created. It is reasonable to assume that the same statement can be made for a DRAM in a spin 1 system in which alignment is the only multipole moment created and detected by the linearly polarized light. For angular momenta  $F > 1$  the creation of higher order ( $k > 2$ ) multipole moments and their transfer back to (detectable)  $k = 2$  moments limits the validity of substitution (11) to low light powers.

## V. RESULTS

The calculation outlined above yields signals  $S_\omega(t)$  and  $S_{2\omega}(t)$  which are modulated at the rf frequency  $\omega$  and at its second harmonic  $2\omega$ , and which can be written as

$$S_\omega(t) = h_\omega(\gamma) [ D_\omega \cos(\omega t - \alpha) - A_\omega \sin(\omega t - \alpha) ], \quad (12a)$$

$$S_{2\omega}(t) = h_{2\omega}(\gamma) [ -A_{2\omega} \cos(2\omega t - 2\alpha) - D_{2\omega} \sin(2\omega t - 2\alpha) ], \quad (12b)$$

where the angular dependence of the signals is given by  $h_\omega(\gamma)$  and  $h_{2\omega}(\gamma)$ . As stated earlier the orientation angle  $\alpha$  of the rf field appears as a phase shift. The in-phase and quadrature components of the signal have both absorptive ( $A_\omega, A_{2\omega}$ ) and dispersive ( $D_\omega, D_{2\omega}$ ) lineshapes given by

$$D_\omega = \frac{\Gamma_0 \omega_1 (\Gamma_2^2 + 4\delta^2 - 2\omega_1^2) \delta}{Z}, \quad (13a)$$

$$A_\omega = \frac{\Gamma_0 \omega_1 [(\Gamma_2^2 + 4\delta^2) \Gamma_1 + \Gamma_2 \omega_1^2]}{Z}, \quad (13b)$$

$$D_{2\omega} = \frac{\Gamma_0 \omega_1^2 (2\Gamma_1 + \Gamma_2) \delta}{Z}, \quad (13c)$$

$$A_{2\omega} = \frac{\Gamma_0 \omega_1^2 (\Gamma_1 \Gamma_2 - 2\delta^2 + \omega_1^2)}{Z}, \quad (13d)$$

with

$$\begin{aligned} Z = & \Gamma_0 (\Gamma_1^2 + \delta^2) (\Gamma_2^2 + 4\delta^2) \\ & + (\Gamma_1 \Gamma_2 (2\Gamma_0 + 3\Gamma_2) - 4\delta^2 (\Gamma_0 - 3\Gamma_1)) \omega_1^2 \\ & + (\Gamma_0 + 3\Gamma_2) \omega_1^4, \end{aligned} \quad (14)$$

Equations (13) and (14) can be simplified substantially if we assume an isotropic relaxation by setting  $\Gamma_0 = \Gamma_1 = \Gamma_2 \equiv \Gamma$ . We will stick to this assumption in the following discussion since it does not change the general properties of the spectra. We further simplify the notation by introducing a dimensionless rf saturation parameter  $S_{\text{rf}} = (\omega_1/\Gamma)^2$  and a

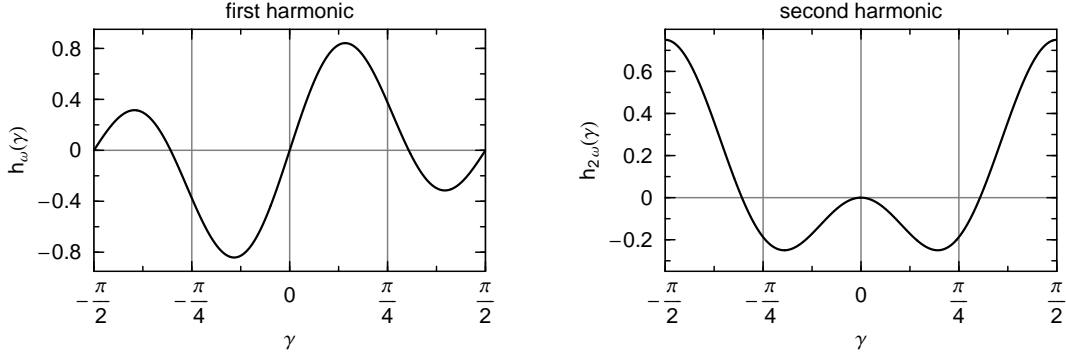


FIG. 3: Angular dependence of the first ( $h_\omega$ , left) and second ( $h_{2\omega}$ , right) harmonic signals on the angle  $\gamma$  between the light polarization  $\epsilon$  and the magnetic offset field  $\mathbf{B}_0$ .

normalized detuning  $x = \delta/\Gamma$ . With these assumptions and definitions we obtain

$$D_\omega(x, S_{\text{rf}}) = \frac{x(1 - 2S_{\text{rf}} + 4x^2)\sqrt{S_{\text{rf}}}}{(1 + S_{\text{rf}} + x^2)(1 + 4S_{\text{rf}} + 4x^2)}, \quad (15a)$$

$$A_\omega(x, S_{\text{rf}}) = \frac{(1 + S_{\text{rf}} + 4x^2)\sqrt{S_{\text{rf}}}}{(1 + S_{\text{rf}} + x^2)(1 + 4S_{\text{rf}} + 4x^2)}, \quad (15b)$$

$$D_{2\omega}(x, S_{\text{rf}}) = \frac{3xS_{\text{rf}}}{(1 + S_{\text{rf}} + x^2)(1 + 4S_{\text{rf}} + 4x^2)}, \quad (15c)$$

$$A_{2\omega}(x, S_{\text{rf}}) = \frac{(1 + S_{\text{rf}} - 2x^2)S_{\text{rf}}}{(1 + S_{\text{rf}} + x^2)(1 + 4S_{\text{rf}} + 4x^2)}. \quad (15d)$$

In the following we will discuss in detail the different properties of the signals (12) with lineshapes (15).

### A. Angular dependencies

The angular dependencies of the first and second harmonic signals (Fig. 3) are given by

$$h_\omega(\gamma) = \frac{3}{2} \sin \gamma \cos \gamma (3 \cos^2 \gamma - 1) \quad (16a)$$

$$\begin{aligned} &= \frac{3}{16} (2 \sin 2\gamma + 3 \sin 4\gamma) \\ &= -\sqrt{6} C_{2,1}(\gamma) C_{2,0}(\gamma) \\ h_{2\omega}(\gamma) &= \frac{3}{4} \sin^2 \gamma (1 - 3 \cos^2 \gamma) \quad (16b) \\ &= \frac{3}{32} (1 - 4 \cos 2\gamma + 3 \cos 4\gamma) \\ &= -\sqrt{6} C_{2,2}(\gamma) C_{2,0}(\gamma) \end{aligned}$$

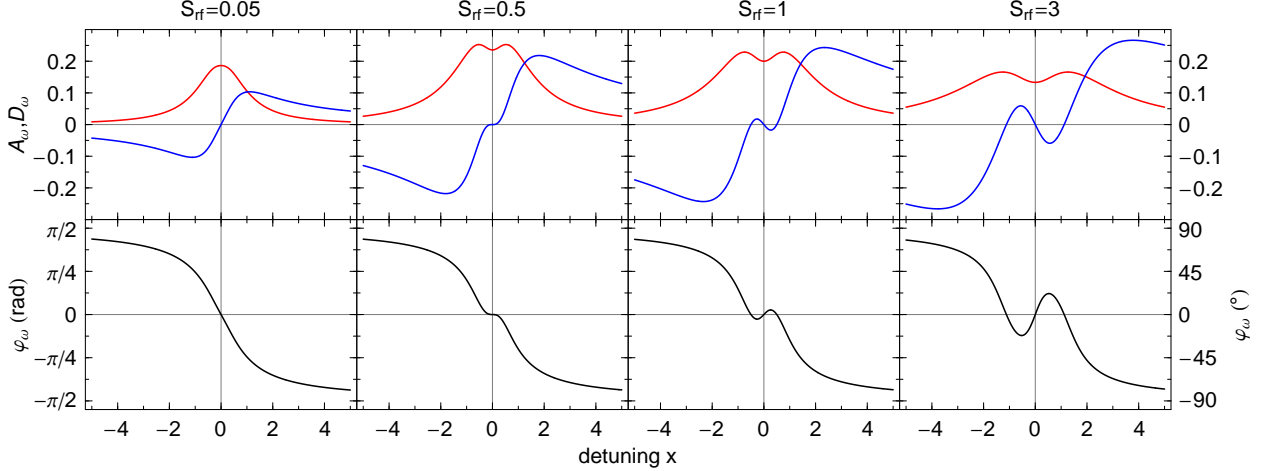


FIG. 4: Top line: Line shapes of the absorptive ( $A_\omega$ ) and dispersive ( $D_\omega$ ) components of the first harmonic signal for different values of the rf saturation parameter  $S_{\text{rf}}$ . Bottom line: Shape of the phase signal  $\varphi_\omega$  for the same values of  $S_{\text{rf}}$ .  $x = (\omega - \omega_0)/\Gamma$  is the normalized detuning of the rf frequency  $\omega$  with respect to the Larmor frequency  $\omega_0$ .

where the  $C_{2,q}$  are the spherical components of the unit alignment tensor along  $\mathbf{B}_0$  in the lab frame. They are related to the spherical harmonics by

$$C_{k,q}(\gamma) = \sqrt{\frac{4\pi}{2k+1}} Y_{k,q}(\gamma, \phi = 0). \quad (17)$$

## B. Line shapes

For low rf intensities, i.e., for  $S_{\text{rf}} \rightarrow 0$ , the lineshapes (15) reduce to

$$D_\omega(x, S_{\text{rf}} \rightarrow 0) = \frac{x}{1+x^2} \sqrt{S_{\text{rf}}}, \quad (18a)$$

$$A_\omega(x, S_{\text{rf}} \rightarrow 0) = \frac{1}{1+x^2} \sqrt{S_{\text{rf}}}, \quad (18b)$$

and

$$D_{2\omega}(x, S_{\text{rf}} \rightarrow 0) = \frac{3x}{(1+x^2)(1+4x^2)} S_{\text{rf}}, \quad (19a)$$

$$A_{2\omega}(x, S_{\text{rf}} \rightarrow 0) = \frac{1-2x^2}{(1+x^2)(1+4x^2)} S_{\text{rf}}. \quad (19b)$$

Expressions (16) and (18), correspond to results obtained in earlier work [7, 8].

The corresponding spectra can be seen in the leftmost columns of Figs. 4 and 5. These figures also show how the lineshapes of the absorptive and dispersive signals  $A_\omega, D_\omega, A_{2\omega}$ ,

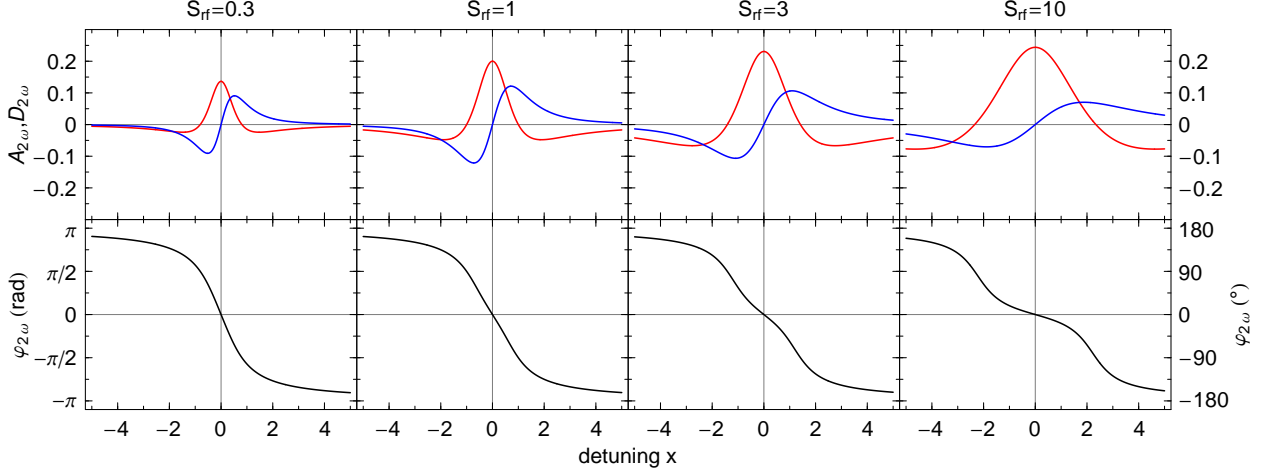


FIG. 5: Top line: Line shapes of the absorptive ( $A_{2\omega}$ ) and dispersive ( $D_{2\omega}$ ) components of the second harmonic signal for different values of the rf saturation parameter  $S_{rf}$ . Bottom line: Shape of the phase signal  $\varphi_{2\omega}$  for the same values of  $S_{rf}$ .

and  $D_{2\omega}$  change with increasing rf intensity. A narrow additional spectral feature appears in the first harmonic signal for  $S_{rf} > 0.5$ . The origin of this structure can be explained as follows: the basic interaction of the rf field with the angular momentum is the coupling of adjacent Zeeman sublevels. The corresponding  $\Delta M = \pm 1$  coherences oscillate at the rf frequency  $\omega$  and their detection by the light field constitutes the first harmonic signal. With increasing rf power, a further interaction of a  $\Delta M = 1$  coherence with the rf field  $B_1$  becomes possible and leads to the creation of a  $\Delta M = 2$  coherence, whose oscillation produces the second harmonic signal. An additional interaction of the  $\Delta M = 2$  coherence with the rf field produces both  $\Delta M = 3$  and  $\Delta M = 1$  coherences. While the former cannot be detected optically since linearly polarized light couples at most to  $\Delta M = 2$  coherences, the latter directly contributes to the first harmonic signal. In this sense, the additional features can be understood as resulting from the creation of a  $\Delta M = 2$  coherence by a second order interaction with the rf field, the evolution of that coherence in the offset field, and back-transfer to a  $\Delta M = 1$  coherence by an additional interaction with the rf field followed by detection of that coherence at the first harmonic frequency  $\omega$ .

The additional narrow feature in the absorptive signal that appears at large rf intensities was already observed in the pioneering work by Colegrove and Franken on optically induced alignment [11]. Based on the results presented above the feature can be explained in terms

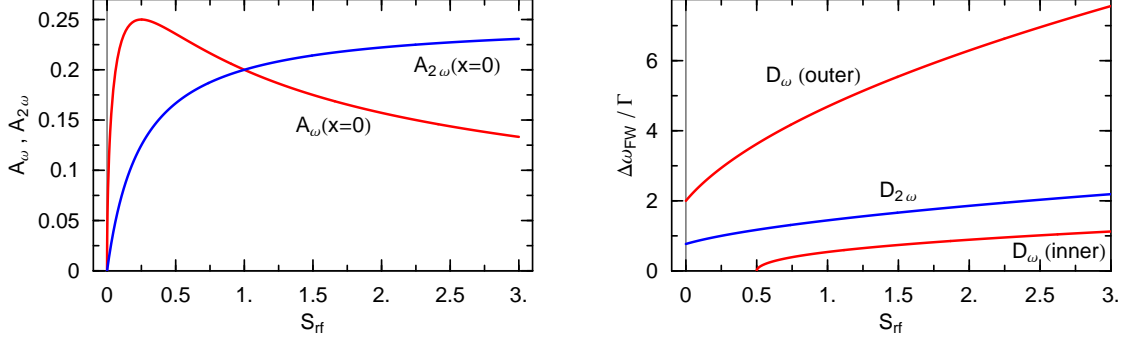


FIG. 6: Saturation of the resonant absorptive signals  $A_\omega$  and  $A_{2\omega}$  (left), and widths of the dispersive signals  $D_\omega$  and  $D_{2\omega}$  as a function of the rf intensity  $S_{\text{rf}}$  (right). Inner and outer refer to the broad and the narrow structures of the first harmonic signals  $D_\omega$ .

of line superpositions. In fact, the expression for the absorptive first harmonic signal  $A_\omega$  (Eq. 15b) can be rewritten as

$$A_\omega = \frac{1 + S_{\text{rf}}}{1 + S_{\text{rf}} + x^2} \sqrt{S_{\text{rf}}} - \frac{4S_{\text{rf}}}{1 + 4S_{\text{rf}} + 4x^2} \sqrt{S_{\text{rf}}}, \quad (20)$$

i.e., as a superposition of two absorptive Lorentzian line shapes whose widths, for  $S_{\text{rf}} \rightarrow 0$ , differ by a factor of 2, while they become equal for large values of  $S_{\text{rf}}$ . The appearance of the central dip is a consequence of the different rates at which the contributions saturate with increasing  $S_{\text{rf}}$ . At low rf powers, the amplitudes of the two contributions to the first harmonic signals (20) grow as  $S_{\text{rf}}^{1/2} \propto \omega_1$  and  $S_{\text{rf}}^{3/2} \propto \omega_1^3$  respectively, which reflects that these resonances correspond to first and third order processes as discussed above. The second harmonic signals (Eqs. 19a, 19b), on the other hand, grow as  $\omega_1^2$ , which reflects their second order nature.

### C. Amplitudes of absorptive and widths of dispersive signals

Let us next consider the amplitudes of the absorptive signals  $A_\omega$  and  $A_{2\omega}$  given by Eqs. 15b and 15d. On resonance, the signal amplitudes are given by

$$A_\omega(x = 0) = \frac{\sqrt{S_{\text{rf}}}}{1 + 4S_{\text{rf}}}$$

$$A_{2\omega}(x = 0) = \frac{S_{\text{rf}}}{1 + 4S_{\text{rf}}}.$$

These dependencies are shown on the left in Fig. 6. The second harmonic signal amplitude saturates, for  $S_{\text{rf}} \rightarrow \infty$ , at a value of  $A_{2\omega}^{\text{max}} = 0.25$ , while the first harmonic signal reaches a maximum  $A_{\omega}^{\text{max}} = 0.25$  at  $S_{\text{rf}} = 0.25$  and vanishes for  $S_{\text{rf}} \rightarrow \infty$ .

The dependence of the line widths, i.e., the frequency separation  $\Delta\omega_{\text{FW}}$  of the maxima and minima of the dispersive signals  $D_{\omega}$  and  $D_{2\omega}$  on  $S_{\text{rf}}$  can be inferred from the derivatives of (15a) and (15c). Although an algebraic expression can be derived for the width of the first harmonic dispersive signal  $D_{\omega}$ , this expression is too complex to be displayed here. We quote only the expression for the rf power broadening of the width of the second harmonic dispersive signal  $D_{2\omega}$ , i.e.,

$$\frac{\Delta\omega_{\text{FW}}^{D_{2\omega}}}{\Gamma} = \frac{1}{\sqrt{6}} \sqrt{\sqrt{73 + 320S_{\text{rf}} + 256S_{\text{rf}}^2} - 5 - 8S_{\text{rf}}}. \quad (21)$$

The results are shown on the right in Fig. 6. Extrapolating the widths to  $S_{\text{rf}} = 0$  yields

$$\begin{aligned} \Delta\omega_{\text{FW}}^{D_{\omega}}(S_{\text{rf}} \rightarrow 0) &= 2\Gamma \\ \Delta\omega_{\text{FW}}^{D_{2\omega}}(S_{\text{rf}} \rightarrow 0) &= \sqrt{\frac{\sqrt{73} - 5}{6}} \Gamma = 0.769\Gamma. \end{aligned}$$

The dispersive line shape of the second harmonic signal  $D_{2\omega}$  is thus 2.6 times narrower than the corresponding first harmonic signal.

## VI. THE PHASE OF THE SIGNALS

We define the phases  $\varphi_{\omega}$  ( $\varphi_{2\omega}$ ) of the first and second harmonic signals as the phase difference between  $S_{\omega}(t)$  ( $S_{2\omega}(t)$ ) and oscillations that are proportional to  $\cos \omega t$  ( $\cos 2\omega t$ ) respectively. This definition is motivated by the fact that the rf field in the lab frame is proportional to  $\cos \omega t$ . As an alternative to the parametrization of the signals in terms of in-phase and quadrature components (Eq. 12) one can write  $S_{\omega}(t)$  and  $S_{2\omega}(t)$  in terms of moduli  $R_{\omega}$ ,  $R_{2\omega}$  and phases  $\varphi_{\omega}$ ,  $\varphi_{2\omega}$  according to

$$S_{\omega} = h_{\omega}(\gamma)R_{\omega}(x, S_{\text{rf}}) \cos[\omega t + \varphi_{\omega}(x, S_{\text{rf}})], \quad (22a)$$

$$S_{2\omega} = h_{2\omega}(\gamma)R_{2\omega}(x, S_{\text{rf}}) \cos[2\omega t + \varphi_{2\omega}(x, S_{\text{rf}})], \quad (22b)$$

with

$$R_\omega = \frac{\sqrt{S_{\text{rf}}(4x^2 + 1)[4x^4 - (4S_{\text{rf}} - 5)x^2 + (S_{\text{rf}} + 1)^2]}}{(x^2 + S_{\text{rf}} + 1)(4x^2 + 4S_{\text{rf}} + 1)},$$

$$R_{2\omega} = S_{\text{rf}} \frac{\sqrt{4x^4 - (4S_{\text{rf}} - 5)x^2 + (S_{\text{rf}} + 1)^2}}{(x^2 + S_{\text{rf}} + 1)(4x^2 + 4S_{\text{rf}} + 1)},$$

and

$$\varphi_\omega = \arctan\left(\frac{A_\omega(x, S_{\text{rf}})}{D_\omega(x, S_{\text{rf}})}\right) - \alpha \quad (23)$$

$$\varphi_{2\omega} = \arctan\left(-\frac{D_{2\omega}(x, S_{\text{rf}})}{A_{2\omega}(x, S_{\text{rf}})}\right) - 2\alpha. \quad (24)$$

A dual-phase lock-in amplifier can be used to extract the  $R$ 's and  $\varphi$ 's from the signal. Such amplifiers usually allow one to apply an offset phase  $\varphi_{\text{os}}$  to the signal which then adds to  $\alpha$ . For stabilization purposes, it is practical to choose that offset phase such that the total phase vanishes at the center of the resonance  $\varphi_\omega(x=0) = \varphi_{2\omega}(x=0) = 0$ . This choice avoids phase discontinuities and provides a signal  $\varphi(x) \propto x$  (for  $x \ll 1$ ) that is proportional to magnetic field changes near the center of the resonance. In the parametrization defined above this can be realized simultaneously for both signals when  $\alpha + \varphi_{\text{os}} = \pi/2$ . In that case the phase signals take the form

$$\varphi_\omega = -\arctan\left(x \frac{1 - 2S_{\text{rf}} + 4x^2}{1 + S_{\text{rf}} + 4x^2}\right), \quad (25a)$$

$$\varphi_{2\omega} = -\arctan\left(\frac{3x}{1 + S_{\text{rf}} - 2x^2}\right). \quad (25b)$$

Examples of  $\varphi_\omega(x)$  and  $\varphi_{2\omega}(x)$  for different values of  $S_{\text{rf}}$  are shown in Figs. 4 and 5 respectively.

The phase of the first harmonic signal  $\varphi_\omega$  (Eq. 25a) for low rf power ( $S_{\text{rf}} \ll 1/2$ ) is identical to the phase of an orientation based magnetic resonance signal (DROM see Sec. IX). Conversely to that DROM phase (34b), which does not depend on  $S_{\text{rf}}$ , the DRAM phases  $\varphi_\omega$  and  $\varphi_{2\omega}$  depend on  $S_{\text{rf}}$ , and  $\varphi_\omega$  even changes the sign of its slope at  $S_{\text{rf}} = 1/2$ . Note that  $\varphi_{2\omega}$  makes a total phase swing of  $2\pi$  across the resonance, while  $\varphi_\omega$  swings only by  $\pi$ .

## VII. PARAMETRIZATION IN $\theta, \phi$ GEOMETRY

A parametrization of the magnetometer signals in terms of the azimuthal and polar angles  $\theta$  and  $\phi$  of Fig. 1 is useful for practical applications in which one may want to rotate the

plane of polarization, i.e., change  $\phi$  only. Using the procedure outlined in section IV one can show that the signals are then given by

$$S_\omega(t) = g_\omega(\theta, \phi) [ A_\omega(x, S_{\text{rf}}) \cos(\omega t - \beta) + D_\omega(x, S_{\text{rf}}) \sin(\omega t - \beta) ] , \quad (26a)$$

$$S_{2\omega}(t) = g_{2\omega}(\theta, \phi) [-A_{2\omega}(x, S_{\text{rf}}) \cos(2\omega t - 2\beta) - D_{2\omega}(x, S_{\text{rf}}) \sin(2\omega t - 2\beta)] , \quad (26b)$$

where the line shape functions  $A_\omega$ ,  $A_{2\omega}$ ,  $D_\omega$ , and  $D_{2\omega}$  correspond to the expressions given by Eq. (15). The phase angle  $\beta$  is given by

$$\beta = \alpha + \arctan\left(\frac{\tan \phi}{\cos \theta}\right) ,$$

while the angular dependencies of the first and second harmonic signals are given by

$$g_\omega(\theta, \phi) = \frac{3}{2} \cos \phi \sin \theta (-1 + 3 \cos^2 \phi \sin^2 \theta) \times \sqrt{1 - \sin^2 \theta \cos^2 \phi} , \quad (27)$$

$$g_{2\omega}(\theta, \phi) = \frac{3}{4} (-1 + 3 \cos^2 \phi \sin^2 \theta) \times (\sin^2 \theta \cos^2 \phi - 1) . \quad (28)$$

Note that the relation  $\cos \gamma = \sin \theta \cos \phi$  holds.

## VIII. MAGNETOMETRY CONSIDERATIONS

There are two modes of OPM operation, the self-oscillating mode and the free running mode, which differ in the way the magnetic field value is extracted from the signals described above. Self-oscillating (or phase stabilized) magnetometers use feedback to keep the driving frequency  $\omega$  equal to  $\omega_0$ , and in such magnetometers,  $\omega$  is measured with a frequency counter [19]. We will not discuss the self-oscillating mode in detail since the feedback is difficult to describe analytically. Instead, we discuss the free-running mode which yields an identical magnetic field sensitivity. The goal of the following discussion is not the derivation of absolute field sensitivities, but rather a comparison of the relative magnetometric sensitivities that one can expect from the first and second harmonic signals.

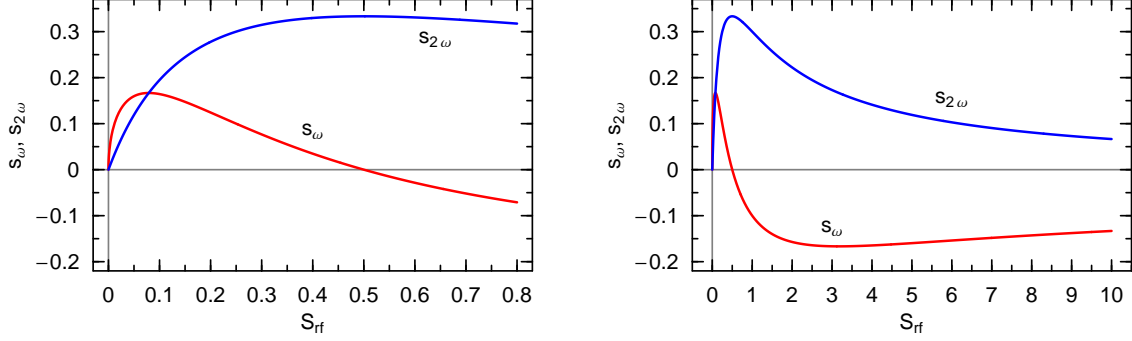


FIG. 7: Slopes  $s_{\omega,2\omega}$  of the dispersive signals on resonance ( $x = 0$ ) as a function of the rf saturation parameter for two different ranges of  $S_{\text{rf}}$ .

As a free-running magnetometer application we consider the recording of signal changes induced by variations of the offset field  $B_0$  while the rf frequency  $\omega$  is kept constant. Either the dispersive signals  $D_\omega$  and  $D_{2\omega}$  (Eqs. 15a,15c) or the phase signals  $\varphi_\omega$  and  $\varphi_{2\omega}$  (Eqs. 25a,25b) can be used as discriminating signals as they both feature a linear dependence on  $B_0$  changes near the center of the resonance ( $x = 0$ ).

The resolution with which field changes can be detected is limited by noise processes such as photon shotnoise, electron shotnoise (in a photodiode), and spin projection noise, all of which have white a noise spectrum. We specify the magnetometric sensitivity in terms of the noise equivalent magnetic field (NEM) [20, 21], which is the amplitude  $\Delta B^{\text{NEM}}$  of field fluctuations which induce fluctuations of the (dispersive) signal  $S(B_0)$  that are equal to the signal noise  $\Delta S$ :

$$\Delta B^{\text{NEM}} = \Delta S (dS/dB_0|_{x=0})^{-1}$$

One can show that for a given noise level of the modulated signal one obtains the same NEM either from the demodulated signal  $S = D_\omega(D_{2\omega})$  or from the demodulated signal  $S = \varphi_\omega(\varphi_{2\omega})$ . The minimal value of  $\Delta B^{\text{NEM}}$  is thus obtained under conditions which maximize  $h_\omega \cdot s_\omega$  and  $h_{2\omega} \cdot s_{2\omega}$ , where the (on resonance) slopes  $s_\omega$  and  $s_{2\omega}$  are given by

$$s_\omega = \left. \frac{dD_\omega}{dx} \right|_{x=0} = \frac{(1 - 2S_{\text{rf}})\sqrt{S_{\text{rf}}}}{(1 + S_{\text{rf}})(1 + 4S_{\text{rf}})}, \quad (29a)$$

$$s_{2\omega} = \left. \frac{dD_{2\omega}}{dx} \right|_{x=0} = \frac{3S_{\text{rf}}}{(1 + S_{\text{rf}})(1 + 4S_{\text{rf}})}. \quad (29b)$$

Figure 7 shows their dependence on the rf intensity. The zero crossing of the slope of the first

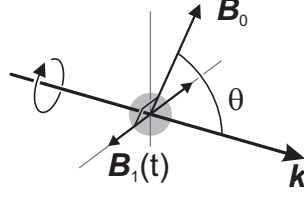


FIG. 8: Geometry of double resonance spectroscopy involving circularly polarized light. The oscillating field  $\mathbf{B}_1$  is perpendicular to the offset field  $\mathbf{B}_0$ .

harmonic signal at  $S_{\text{rf}} = 0.5$  marks the emergence of the narrow central feature in Fig. 5.

The maximal sensitivity (minimal  $\Delta B_{\omega, 2\omega}^{\text{NEM}}$ ) is achieved by choosing a geometry which maximizes  $h_\omega$  and  $h_{2\omega}$  and an rf intensity, which maximizes  $s_\omega$  and  $s_{2\omega}$ . For the first harmonic signal one finds  $\max[h_\omega \cdot s_\omega] = 0.141$  for  $\gamma=25.5^\circ$  and  $S_{\text{rf}}=0.079$ , while for the second harmonic signal one has  $\max[h_{2\omega} \cdot s_{2\omega}] = 0.25$  for  $\gamma=90^\circ$  and  $S_{\text{rf}}=0.5$ . Under optimized geometrical and rf power conditions and for a given noise level the second harmonic signal is thus expected to yield a 1.8 times higher sensitivity to magnetic field changes than the first harmonic signal.

## IX. DROM SIGNALS

Although detailed line shapes for magnetometers based on circularly polarized radiation have been discussed in detail in the literature [3] we quote the corresponding expressions here for completeness. We discuss again only geometries in which  $B_1$  is perpendicular to  $B_0$ , described by a single angular variable  $\theta$  (Fig. 8). Optical pumping with circularly polarized light creates a longitudinal orientation  $m_{1,0}^{\text{ini}}$

$$m_{1,0}^{\text{ini}} = N_1(F) \sum_{M=-F}^F p_M M$$

along the laser beam direction, which we defines the quantization axis in the lab frame. Relaxation leads to an equilibrium orientation  $m_{1,0}^{\text{eq}} = m_{1,0}^{\text{ini}} \cos \theta$  along the magnetic field. The oscillating orientation components  $m_{1,q}$  are obtained by solving the Bloch equations (8) in the rw frame, and the corresponding expressions in the lab frame are obtained by the back rotations in a similar way as discussed in section IV. One can show that the absorption

coefficient for circularly polarized light by an oriented medium is given by

$$\kappa \propto \frac{A_0}{\sqrt{3}} m_{0,0} - \sqrt{\frac{1}{2}} A_1 m_{1,0}, \quad (30)$$

where  $m_{1,0}$  is defined for a quantization axis along  $\hat{k}$ . Defining the DROM signal, in analogy with (10), as

$$S_\omega(t) = \frac{m_{1,0}(t)}{m_{1,0}^{\text{ini}}} = f_\omega(\theta) (d_\omega \cos \omega t - a_\omega \sin \omega t), \quad (31)$$

the dispersive and absorptive line shapes are given by

$$d_\omega = d_\omega(x, S_{\text{rf}}) = \frac{x}{1 + S_{\text{rf}} + x^2} \sqrt{S_{\text{rf}}}, \quad (32a)$$

$$a_\omega = a_\omega(x, S_{\text{rf}}) = \frac{1}{1 + S_{\text{rf}} + x^2} \sqrt{S_{\text{rf}}}, \quad (32b)$$

with the angular dependence

$$f_\omega(\theta) = \frac{1}{\sqrt{2}} \cos \theta \sin \theta = -C_{1,1}(\theta) C_{1,0}(\theta), \quad (33)$$

where  $C_{1,q}(\theta)$  is given by Eq. 17. The modulus  $r_\omega$  and the phase of the DROM signal, defined in analogy to (25), are given by

$$r_\omega = \frac{\sqrt{1 + x^2}}{1 + S_{\text{rf}} + x^2} \sqrt{S_{\text{rf}}}, \quad (34a)$$

$$\varphi_\omega^{\text{DROM}}(x) = -\arctan x. \quad (34b)$$

We recall that the given signals are again valid for arbitrary spin systems in the low laser power limit.

## X. SUMMARY AND CONCLUSION

We have presented a general theoretical framework for the calculation of optical rf double resonance signals that can be easily applied to oriented or aligned atomic media. The theory yields analytical results with a broad range of validity, and is only limited by the assumption of low light power.

DRAMs, i.e., magnetometers that use linearly polarized light, present several potential advantages over the well known DROM scheme:

- **Line widths:** The line shapes of the second harmonic DRAM signal have significantly narrower linewidths than the DROM signal under identical conditions. Narrow

linewidths potentially increase the magnetometric sensitivity and suppress systematic errors in optical magnetometers due to long term baseline drifts [22].

- Light shift: In DROM devices the interaction of the atoms with the circularly polarized laser light leads to  $M$  dependent energy shifts (vector light shift) of the sublevels  $|F, M\rangle$  when the laser frequency is not centered on the optical resonance line. In that case, power and frequency fluctuations of the laser mimic magnetic field fluctuations, thereby limiting the magnetometric performance. In the DRAM device the linearly polarized light produces a tensor light shift [23] depending on  $M^2$ , which does not have the characteristics of the Zeeman interaction and will therefore not affect the magnetometric performance.
- Geometry: The DROM scheme achieves a maximal sensitivity for  $\theta = \pi/4$  (Eq. 33). The  $45^\circ$  angle that the laser beam has to make with the magnetic field seriously limits applications which call for a compact arrangement of multiple sensors. In multi-channel devices, as required, e.g., for cardiomagnetic measurements [24], the use of the DRAM signals offers the advantage that the laser beam can be oriented either parallel or perpendicular to the offset field.
- Vector magnetometry: Both the DROM and the DRAM devices are scalar magnetometers and their resonance frequency measures  $|B_0|$ . However, the DRAM signals can be used to realize a vector magnetometer, since the ratio of  $R_{2\omega}/R_\omega$  is proportional to  $\tan \gamma$ , for all values of  $S_{\text{rf}}$ . The knowledge of  $|\mathbf{B}_0|$  and  $\gamma$  locates  $\hat{B}_0$  on a cone and the variation of the signal with  $\phi$ , obtained by rotating the polarizer, will determine the polar angle of  $\hat{B}_0$  on the cone. In this way the DRAM scheme can be used to infer all three vector components of the field.
- Relaxation: We are in the process of performing extensive experimental studies of the DRAM properties in paraffine coated cesium cells [25]. First results indicate that a description of the signals using three independent relaxation rates (Eqs. 13) is required to describe the experimental lineshapes in detail. The DRAM signals thus seem to offer a convenient way for studying spin relaxation processes in aligned media.
- Signal noise: Diode lasers are convenient light sources for double resonance experiments. However, they often feature a  $1/f$  (flicker) intensity noise at low frequencies

that turns into the white shot noise level at higher frequencies. The detection of  $D_{2\omega}$  and  $A_{2\omega}$  at twice the Larmor frequency makes it easier to operate in a region where the laser noise is less affected by flicker noise.

Cs OPMs in the DROM geometry have a shot noise limited sensitivity of  $10 \text{ fT/Hz}^{1/2}$  [21]. A direct experimental comparison of DRAM and DROM magnetometers is currently underway in our laboratory. This study will show if the potential advantages can be realized in practice.

### Acknowledgments

The authors thank P. Knowles, A. Pazgalev, and G. Di Domenico for useful discussions and a critical reading of the manuscript. This work was supported by grant Nr. 205321-105597 from the Swiss National Science Foundation and by grant Nr. 8057.1 LSPP-LS from the Swiss Innovation Promotion Agency, CTI.

- 
- [1] J. Brossel and F. Bitter, *Phys. Rev.* **86** (3), 308 (1952).
  - [2] A. L. Bloom, *Appl. Opt.* **1**, 61 (1962).
  - [3] E. B. Alexandrov and V. A. Bonch-Bruevich, *Opt. Eng.* **31**, 711 (1992).
  - [4] H. G. Dehmelt, *Phys. Rev.* **105** (5), 1924 (1957).
  - [5] B. S. Mathur, H. Y. Tang, and W. Happer, *Phys. Rev. A* **2**, 648 (1970).
  - [6] W. E. Bell and A. L. Bloom, *Phys. Rev. Lett.* **6**, 623 (1961).
  - [7] H. Gilles, B. Cheron, and J. Hamel, *J. Phys. II France* **2**, 781 (1992).
  - [8] B. Cheron, H. Gilles, J. Hamel, O. Moreau, and E. Noël, *J. Phys. III France* **7**, 1735 (1997).
  - [9] K. Blum, *Density Matrix Theory and Applications* (Plenum Press, New York, 1996).
  - [10] W. Happer, *Rev. Mod. Phys.* **44**, 169 (1972).
  - [11] F. D. Colegrove and P. A. Franken, *Phys. Rev.* **119** (2), 680 (1960).
  - [12] E. B. Aleksandrov and M. V. Balabas, *Opt. Spectrosc.* **69**, 4 (1990).
  - [13] H. Gilles, J. Hamel, and B. Cheron, *Rev. Sci. Instr.* **72**, 2253 (2001).
  - [14] D. Budker, D. F. Kimball, V. V. Yashchuk, and M. Zolotarev, *Phys. Rev. A* **65**, 055403 (2002).

- [15] D. Budker, D. F. Kimball, S. M. Rochester, V. V. Yashchuk, and M. Zolotarev, *Phys. Rev. A* **62**, 043403 (2000).
- [16] D. Budker, W. Gawlik, D. F. Kimball, S. M. Rochester, V. V. Yashchuk, and A. Weis, *Rev. Mod. Phys.* **74**, 1153 (2002).
- [17] W. Happer, *Phys. Rev. B* **1**, 2203 (1970).
- [18] N. Tsukada, T. Yabuzaki, and T. Ogawa, *J. Phys. Soc. Jap.* **11**, 698 (1972).
- [19] S. Groeger, G. Bison, P. E. Knowles, and A. Weis, *Eur. Phys. J. Appl. Phys.* **33**, 221 (2006).
- [20] G. Bison, R. Wynands, and A. Weis, *J. Opt. Soc. Am. B.* **22**, 77 (2005).
- [21] S. Groeger, G. Bison, J.-L. Schenker, R. Wynands, and A. Weis, *Eur. Phys. J. D* **38**, 239 (2006).
- [22] E. B. Alexandrov, A. S. Pazgalev, and J. L. Rasson, *Opt. Spectrosc.* **82**, 14 (1997).
- [23] B. Mathur, H. Tang, and W. Happer, *Phys. Rev.* **171**, 11 (1968).
- [24] G. Bison, R. Wynands, and A. Weis, *Opt. Expr.* **11**, 904 (2003).
- [25] G. Di Domenico et al., to be published (2006).